JOURNAL OF AIRCRAFT
Vol. 31, No. 5, Sept.–Oct. 1994

Buckling Analysis of Geodesically Stiffened Composite Panels with Discrete Stiffeners

Zafer Gürdal* and Bruno Grall†
Virginia Polytechnic Institute and State University, Blacksburg, Virginia 24061

A computationally efficient analysis is developed to predict the buckling loads of geodesically stiffened composite panels with discrete plate-like stiffeners under in-plane loads. The procedure accounts for the contribution of the in-plane extensional and out-of-plane bending stiffnesses of the stiffeners through the use of a Lagrange multipliers technique in an energy method solution. The analysis is capable of predicting the buckling loads of grid-stiffened panels for a variety of stiffener aspect ratios and stiffener laminate stacking sequences. It can also be used to design panels with variable density grid stiffeners across the panel width. Results of the proposed analysis showed that the buckling loads of geodesically stiffened panels are predicted more accurately, especially in the case of panels with shallow stiffeners, compared to an earlier analysis that assumes the stiffeners to be beam-like components. For plate-like stiffeners, laminate stacking sequence of the stiffeners is found to have a substantial effect on the critical load of a panel. It was demonstrated that the optimal stiffener is not always unidirectional, and tailoring the stiffener ply sequence can lead to improvement in panel stability. It was also shown that panels with a variable grid density can lead to designs with improved buckling performance compared to uniform density panels.

I. Introduction

WITH the introduction of advanced manufacturing processes for high-performance composite materials, it is possible to use these lightweight materials in primary load carrying structures such as the fuselage and wing-box of an aircraft. Various nonaerospace industries can also obtain the benefits of reduced assembly cost from the automated manufacturing of complex stiffening arrangements in flat and cylindrical components through the use of filament winding and tow-placement techniques. Panels that have a grid of stiffeners with a prescribed uniform pattern, such as geodesically stiffened panels, are promising structural components since they permit low-cost fabrication through such automated manufacturing techniques, and are expected to have superior performance characteristics under combined loadings compared to the ring and longitudinally stiffened shells. Moreover, by going to different stiffening arrangements, the response of these panels can be tailored to meet various design requirements.

Analysis of a stiffened structure with a complex grid pattern can be quite difficult. Different computational techniques can be used during the design analysis of such panels. For example, in Ref. 1, a mathematical optimization program coupled with the finite element method is used for the design optimization of geodesically stiffened shells under combined loads. However, the use of the finite element method can become prohibitively expensive due to the large number of analyses that are needed during an optimization run. Also, in order to vary the density of the grid in a panel during an optimization run, positions of some of the stiffeners must be used as design variables. Use of variables that change the configuration of the panel would require expensive remeshing of the finite element model of the structure (at least once per analysis call from the optimizer), and is only applied in cases for which the design cost is not a significant restriction. An alternative to the finite element method is to use computationally efficient analytical techniques, such as the application of energy based methods, for the analysis.

Energy methods are commonly used in the buckling analysis of flat unstiffened panels where the buckled shape of the panel is approximated by a Fourier series. The values of the coefficients of the series, corresponding to the buckling mode shape, are calculated by minimizing the total potential energy. A similar approach can be used in the case of panels stiffened by discrete plate-like stiffeners. In addition to the skin deformations, assumed forms for the stiffener deformations can be expressed in a Fourier series to enable determination of the buckling load and the mode shape. This is done by minimizing the total potential energy of the entire panel while maintaining certain compatibility conditions between the skin and stiffener deformation shapes. Such an approach has recently been used in Ref. 2 to determine buckling loads of grid-stiffened panels. In Ref. 2 the stiffeners are assumed to be beam-like, and only the stiffener bending stiffnesses in a direction perpendicular to the skin are considered. Continuity of the skin and stiffener deformations at selected locations along the length of the stiffeners are imposed via the Lagrange multiplier technique.

The objectives of the present work are twofold. First, an improvement in the analysis procedure described in Ref. 2 is sought by assuming the stiffeners to be plate elements instead of beam elements. Consequently, the stiffener out-of-plane deformation is included as a new degree of freedom (DOF). This additional DOF requires an additional constraint. This constraint is provided by enforcing the continuity of rotation between the skin and the plate stiffeners at their base. The second objective of the present work is to expand the scope of the design configurations studied earlier by allowing the stiffener locations to be variable, thereby allowing designers to achieve more optimal configurations under various loadings.

II. Analysis

In order to simplify the structural analysis of stiffened panels without being too restrictive, several assumptions were made regarding the panel geometry. Each panel consists of a lam-

Received March 6, 1993; revision received Nov. 18, 1993; accepted for publication Nov. 18, 1993.

*Associate Professor, Department of Engineering Science and Mechanics. Associate Fellow AIAA.

†Graduate Student, Department of Engineering Science and Mechanics.

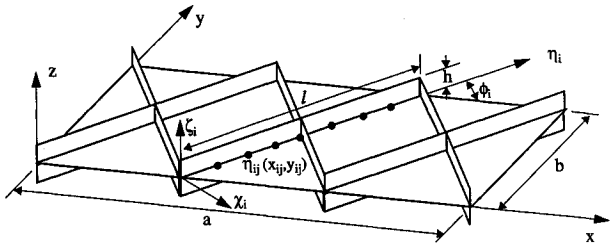

Fig. 1 Panel geometry and stiffener arrangements.

inated skin stiffened with an integral grid of stiffeners, each with a rectangular cross section. The skin is symmetrically laminated and the stiffeners are located on both sides of the skin (see Fig. 1), symmetrically placed about the midplane. This restriction is made to eliminate potential bending-extension coupling in the panel. The analysis presented here can easily be modified to assume the stiffeners to be placed only on one side of the skin. However, one must still assume no bending-extension coupling in order for the linear buckling analysis to be meaningfully applicable. The skin and stiffeners are also assumed to be made of a balanced laminate to eliminate their potential shear-extension coupling. To eliminate shear-extension coupling in the panel, oblique stiffeners are placed in pairs oriented at equal but opposite angles ϕ, with respect to the panel coordinate axes.

The stiffeners considered are currently limited to be laminated plates. Stiffeners with more complicated shapes, such as hat stiffeners, can be studied provided that equivalent A, B, and D matrices can be determined. In the present study, the skin and stiffeners are to be connected in order to obtain a single system of plates. The buckling study applies, therefore, to the panel as a whole and not to each one of its constituents independently.

A. Stability Analysis of Panels

The critical loads of geodesically stiffened panels were calculated in Ref. 2 by using the Rayleigh-Ritz method coupled with a Lagrange multiplier technique. The method requires computation of the total potential energy of the various components of the panel. The following expression for the total potential energy of the skin was derived in Ref. 2 [note that due to a typographical error, the terms $w_{,x}$ and $w_{,y}$ in the load potential are erroneously shown as $w_{,xx}$ and $w_{,yy}$ in Eq. (2) of Ref. 2]:

$$\Pi_{\text{skin}} = U + V$$

$$U = \sum_{m=1}^{M}\sum_{n=1}^{N} A_{mn}^2 P^{mn} \tag{1}$$

$$V = -\lambda\left(\sum_{m=1}^{M}\sum_{n=1}^{N} A_{mn}^2 R^{mn} + \sum_{m=1}^{M}\sum_{n=1}^{N}\sum_{p=1}^{M}\sum_{q=1}^{N} A_{mn}A_{pq}S^{mnpq}\right)$$

based on the following assumed form of the out-of-plane mode shape:

$$w(x, y) = \sum_{m=1}^{M}\sum_{n=1}^{N} A_{mn} \sin\frac{m\pi x}{a} \sin\frac{n\pi y}{b} \quad \begin{matrix} 0 \le x \le a \\ 0 \le y \le b \end{matrix} \tag{2}$$

where a and b are the dimensions of the skin along the x and y coordinates, respectively, A_{mn} are the undetermined mode shape coefficients of the skin, and the coefficients P^{mn}, R^{mn}, and S^{mnpg} are given in Appendix A.

1. *Stiffener Potential Energy*

Instead of considering the stiffeners as beams, as was done in Ref. 2, they are considered here to be plates. In the previous study, deformation of the stiffeners in their out-of-plane direction was not taken into account because only the flexural contribution in the skin out-of-plane direction was included. Since the previously obtained optimum designs contain stiffeners with heights 15–20 times larger than their thicknesses,[2] the beam assumption may not be valid. In addition to increasing the accuracy, modeling the stiffeners as plate segments would allow us to evaluate the effects of stiffener lamination sequence on the buckling response of these panels.

Let η be the longitudinal axis of a stiffener, ζ its transverse axis, χ its out-of-plane axis (see Fig. 1), and u, v, w the three corresponding displacements. Assuming that cross-sectional planes remain plane and normal to the stiffener axis as the stiffener bends in its own plane (see, e.g., Ref. 3), we have

$$u(\eta, \zeta) = u_0(\eta) - \zeta\frac{\partial v_0(\eta)}{\partial \eta} \tag{3}$$

Moreover, for small displacements we assume

$$v(\eta, \zeta) = v_0(\eta) \tag{4}$$

where u_0 and v_0 are the displacements at $\zeta = \chi = 0$, i.e., the base of the stiffener.

Complete derivation of the strain energy of a general laminated plate, starting with the Kirchhoff displacement-strain relations, is given by Whitney in Ref. 4. In the case of a symmetric, balanced, and specially orthotropic plate, the strain energy is given by

$$\begin{aligned} U = \frac{1}{2}\int_0^l \Bigg\{ &\int_{-h-(t_s/2)}^{-(t_s/2)} + \int_{(t_s/2)}^{h+(t_s/2)} [A_{11}u_{,\eta}^2 + 2A_{12}u_{,\eta}v_{,\zeta} \\ &+ A_{22}v_{,\zeta}^2 + A_{66}(u_{,\zeta} + v_{,\eta})^2]\, d\zeta \Bigg\} d\eta \\ &+ \frac{1}{2}\int_0^l \Bigg[\int_{-h-(t_s/2)}^{-(t_s/2)} + \int_{(t_s/2)}^{h+(t_s/2)} (D_{11}w_{,\eta\eta}^2 + 2D_{12}w_{,\eta\eta}w_{,\zeta\zeta} \\ &+ D_{22}w_{,\zeta\zeta}^2 + 4D_{66}w_{,\eta\zeta}^2)\, d\zeta \Bigg] d\eta \end{aligned} \tag{5}$$

where l and h are the length and the height of the stiffener, respectively (see Fig. 1), and t_s is the thickness of the skin. Substituting Eqs. (3) and (4) into Eq. (5), the strain energy of a stiffener reduces to

$$\begin{aligned} U = \frac{1}{2}\int_0^l \Bigg\{ &\int_{-h-(t_s/2)}^{-(t_s/2)} + \int_{(t_s/2)}^{h+(t_s/2)} [A_{11}(u_{0,\eta}^2 + \zeta^2 v_{0,\eta\eta}^2 \\ &- 2\zeta u_{0,\eta}v_{0,\eta\eta})]\, d\zeta \Bigg\} d\eta + \frac{1}{2}\int_0^l \Bigg[\int_{-h-(t_s/2)}^{-(t_s/2)} \\ &+ \int_{(t_s/2)}^{h+(t_s/2)} (D_{11}w_{,\eta\eta}^2 + 2D_{12}w_{,\eta\eta}w_{,\zeta\zeta} + D_{22}w_{,\zeta\zeta}^2 \\ &+ 4D_{66}w_{,\eta\zeta}^2)\, d\zeta \Bigg] d\eta \end{aligned} \tag{6}$$

where all the terms in the first integral, other than the one with the coefficient A_{11}, vanish.

The term

$$-2\zeta u_{0,\eta}v_{0,\eta\eta} \tag{7}$$

in Eq. (6) is odd with respect to ζ and, therefore, vanishes during the integration. Moreover, the term

$$A_{11}u_{0,\eta}^2 \tag{8}$$

is independent of the coordinates v and w, and can be considered as an arbitrary constant during out-of-plane and in-plane bending. After eliminating these two terms, two kinds

of terms appear in Eq. (6). Some of the terms are related to the in-plane bending (bending in the plane of the stiffener, but out-of-plane with respect to the skin); others are due to the out-of-plane bending of the stiffener (in the in-plane direction of the skin). Small displacement theory permits us to write the total strain energy of the stiffeners as the sum of energy due to in-plane bending and energy due to out-of-plane deformation.

In the case of a stiffener made of unidirectional material oriented along the longitudinal axis, it is possible to rewrite the in-plane energy term as

$$\frac{1}{2}\int_0^l \left[\int_{-h-(t_s/2)}^{-(t_s/2)} + \int_{(t_s/2)}^{h+(t_s/2)} A_{11}\zeta^2 v_{0,\eta\eta}^2 \, d\zeta\right] d\eta = \frac{E_A I_s}{2}\int_0^l v_{0,\eta\eta}^2 \, d\eta \tag{9}$$

with

$$I_s = 2\left[\frac{t_r h^3}{12} + t_r h\left(\frac{h}{2} + \frac{t_s}{2}\right)^2\right] \tag{10}$$

where t_r is the stiffener thickness, and I_s and E_1 are the moment of inertia and the longitudinal elastic modulus of the stiffener, respectively. The out-of-plane part of the energy expression is the same as the one used in Ref. 2.

Potential energy of the uniform axial loading N applied along the short edges of the stiffener is derived next. The expression for the end shortening $s(\zeta)$ due to the displacements v and w is given by (see, e.g., Ref. 3)

$$s(y) = -\frac{1}{2}\int_0^l \left(\frac{\partial w}{\partial \eta}\right)^2 d\eta - \frac{1}{2}\int_0^l \left(\frac{\partial v_0}{\partial \eta}\right)^2 d\eta \tag{11}$$

where $w = w(\eta, \zeta)$ and $v_0 = v_0(\eta)$. The potential energy of the applied load is therefore

$$V = -W(N) = -\left[\int_{-h-(t_s/2)}^{-(t_s/2)} + \int_{(t_s/2)}^{h+(t_s/2)} s(\zeta) N \, d\zeta\right] = N\left\{\int_{-h-(t_s/2)}^{-(t_s/2)} + \int_{(t_s/2)}^{h+(t_s/2)} \left[-\frac{1}{2}\int_0^l \left(\frac{\partial w}{\partial \eta}\right)^2 - \left(\frac{\partial v_0}{\partial \eta}\right)^2 d\eta\right] d\zeta\right\} \tag{12}$$

We now define the shape functions for the stiffener in-plane and out-of-plane deformations $v_0(\eta)$ and $w(\eta, \zeta)$, respectively. Note that $v_0(\eta)$ is to be connected to the out-of-plane deformation of the skin, which is described by a double Fourier series of Eq. (2). We, therefore, also assume a simple Fourier series to describe $v_0(\eta)$ of the stiffener

$$v_0(\eta) = \sum_{k=1}^{K} B_k \frac{k\pi\eta}{l} \qquad 0 \le \eta \le l \tag{13}$$

where B_k are the undetermined coefficients. This shape function satisfies the geometric boundary conditions at the ends of the stiffeners:

$$\begin{aligned} v_0 &= 0 \quad \text{at} \quad \eta = 0 \\ v_0 &= 0 \quad \text{at} \quad \eta = l \end{aligned} \tag{14}$$

The shape function for the stiffener out-of-plane deflection is slightly more complicated. The stiffeners are attached to the skin along their longitudinal axes, and their out-of-plane deformation corresponds to the in-plane deformation of the skin. In this study, the contribution of the in-plane deformation of the skin is ignored. Therefore, it is assumed for the stiffeners that $w = 0$ at $\zeta = 0$ for all η. The other long edge of each stiffener is free, and the two short edges are assumed to be simply supported. The following shape function satisfies these boundary conditions:

$$w(\eta, \zeta) = \sum_{t=1}^{T}\sum_{k=1}^{K'} C_{tk}\zeta^t \sin\frac{k\pi\eta}{l} \qquad \begin{cases} 0 \le \eta \le l \\ -h - \dfrac{t_s}{2} \le \zeta \le h + \dfrac{t_s}{2} \end{cases} \tag{15}$$

where C_{tk} are the undetermined coefficients. For a panel that has I number of stiffeners, the shape functions $v_0(\eta)$ and $w(\eta, \zeta)$ have to be indexed further to indicate the stiffener number. For the ith stiffener, the displacements are $v_{0i}(\eta)$ and $w_i(\eta, \zeta)$, the undetermined shape coefficient for the displacements are B_{ik} and C_{itk}, respectively, and the length of the stiffener is l_i, where $i = 1, \ldots, I$. The expression for the total potential energy of the stiffeners is the sum of the individual total energies

$$\Pi_{\text{grid}} = \sum_{i=1}^{I} \Pi_{\text{stiff}\,i} \tag{16}$$

2. Total Energy of the Panel

The total potential energy of the panel is the sum of the total potential energies of the skin and stiffeners

$$\Pi_{\text{panel}} = \Pi_{\text{skin}} + \Pi_{\text{grid}} = U_{\text{skin}} + V_{\text{skin}} + U_{\text{grid}} + V_{\text{grid}} \tag{17}$$

By substituting the expressions for the deformation patterns into the individual energy terms it can be shown that

$$\begin{aligned} U_{\text{skin}} &= \sum_{m=1}^{M}\sum_{n=1}^{N} A_{mn}^2 P^{mn} \\ V_{\text{skin}} &= -\lambda\left(\sum_{m=1}^{M}\sum_{n=1}^{N} A_{mn}^2 R^{mn} + \sum_{m=1}^{M}\sum_{n=1}^{N}\sum_{p=1}^{M}\sum_{q=1}^{N} A_{mn}A_{pq}S^{mnpq}\right) \\ U_{\text{grid}} &= \sum_{i=1}^{I}\sum_{t=1}^{T}\sum_{p=1}^{L}\sum_{k=1}^{K'} C_{itk}C_{ipk}U^{itkp} + \sum_{i=1}^{I}\sum_{k=1}^{K} B_{ik}^2 Q^{ik} \\ V_{\text{grid}} &= -\lambda\left(\sum_{i=1}^{I}\sum_{t=1}^{T}\sum_{p=1}^{L}\sum_{k=1}^{K'} C_{itk}C_{ipk}V^{itkp} + \sum_{i=1}^{I}\sum_{k=1}^{K} B_{ik}^2 T^{ik}\right) \end{aligned} \tag{18}$$

where the coefficients P^{mn}, R^{mn}, S^{mnpq}, U^{itkp}, Q^{ik}, V^{itkp}, and T^{ik} are given in Appendix A, and λ is the load factor.

B. Skin-Stiffener Connectivity

So far, the only requirement for the buckling mode shapes of the skin and stiffeners was the compatibility of the modes with the kinematic boundary conditions. Otherwise, the skin and the stiffener mode shapes are completely independent of one another. If the panel is to be treated as a single system, we need to impose additional requirements to enforce compatibility of the skin and stiffener mode shapes. The following sections describe the important compatibility conditions used in the present work.

1. Constraint on the Continuity of Displacement

Compatibility of the out-of-plane deformation pattern of the skin w_{skin}, and the in-plane deformation patterns of the stiffeners v_{0i}, is one of the conditions that must be satisfied. This constraint is enforced at preselected points along the stiffener axes (Fig. 1). Let x, y, and z be the axes of the skin and η, ζ, and χ, the axes of the stiffeners along the longitudinal, transverse, and through-the-thickness directions, re-

spectively. If there are I number of stiffeners, each having a J number of constraint points along their length, then at every constraint point ij, defined by coordinates $(\eta_{ij}, 0, 0)$ for the stiffeners and $(x_{ij}, y_{ij}, 0)$ for the skin, we have the following constraint relation:

$$g_{ij} = \sum_{m=1}^{M}\sum_{n=1}^{N} A_{mn} \sin\frac{m\pi x_{ij}}{a} \sin\frac{n\pi y_{ij}}{b} - \sum_{k=1}^{K} B_{ik} \sin\frac{k\pi\eta_{ij}}{l_i} = 0 \quad \begin{cases} i = 1, 2, \ldots, I \\ j = 1, 2, \ldots, J \end{cases} \tag{19}$$

Note that this constraint is exactly the same as the one used in Ref. 2.

2. Constraint on the Continuity of the Rotation

One of the objectives of the present work is to extend the analysis capability such that compatibility of the skin and stiffener rotations along the lines of stiffener attachment can be enforced. This is again achieved by imposing the constraint at discrete points along each of the stiffeners such that a right angle is maintained between the stiffener and the skin (Fig. 2). If the angle between a stiffener and the x axis of the skin is ϕ_i, the slope of the skin deformation in a direction perpendicular to the stiffener direction ϕ_i can be obtained by using the chain rule of differentiation

$$\frac{\partial}{\partial\chi} = \frac{\partial x}{\partial\chi}\frac{\partial}{\partial x} + \frac{\partial y}{\partial\chi}\frac{\partial}{\partial y} \tag{20}$$

where

$$\frac{\partial x}{\partial\chi} = \sin\phi_i \quad \text{and} \quad \frac{\partial y}{\partial\chi} = -\cos\phi_i \tag{21}$$

For those points along the ith stiffener, the skin slope about the stiffener axis is given by

$$\frac{\partial w_{\text{skin}}}{\partial_{\chi i}} = \sum_{m=1}^{M}\sum_{n=1}^{N} A_{mn}\left(\frac{m\pi}{a}\sin\phi_i\cos\frac{m\pi x}{a}\sin\frac{n\pi y}{b} - \frac{n\pi}{b}\cos\phi_i\sin\frac{m\pi x}{a}\cos\frac{n\pi y}{b}\right) \tag{22}$$

For the slope of the stiffener out-of-plane deformation, using the first derivative of the shape function with respect to the axis ζ, evaluated at $\zeta = 0$, yields the following:

$$h_{ij} = \frac{\partial w_{\text{skin}}}{\partial_{\chi i}}(x_{ij}, y_{ij}) + \frac{\partial w_{\text{stiff}\,i}}{\partial\zeta_i}(\eta_{ij}, 0) = 0 \tag{23}$$

or

$$h_{ij} = \sum_{m=1}^{M}\sum_{n=1}^{N} A_{mn}\left(\frac{m\pi}{a}\sin\phi_i\cos\frac{m\pi x_{ij}}{a}\sin\frac{n\pi y_{ij}}{b} - \frac{n\pi}{b}\cos\phi_i\sin\frac{m\pi x_{ij}}{a}\cos\frac{n\pi y_{ij}}{b}\right) + \sum_{k=1}^{k'} C_{ilk}\sin\frac{k\pi\eta_{ij}}{l_i} = 0 \tag{24}$$

In Eq. (24) the index t of Eq. (15) for the number of terms in transverse direction of the stiffener out-of-plane deformation shape is taken to be 1. This reduction simplifies the calculations significantly, and it is also found to have no significant effect on the calculated buckling loads. That is, linear variation of the out-of-plane deflection of the stiffeners in the transverse direction was found to be appropriate[5] for the modeling of the stiffener mode shapes.

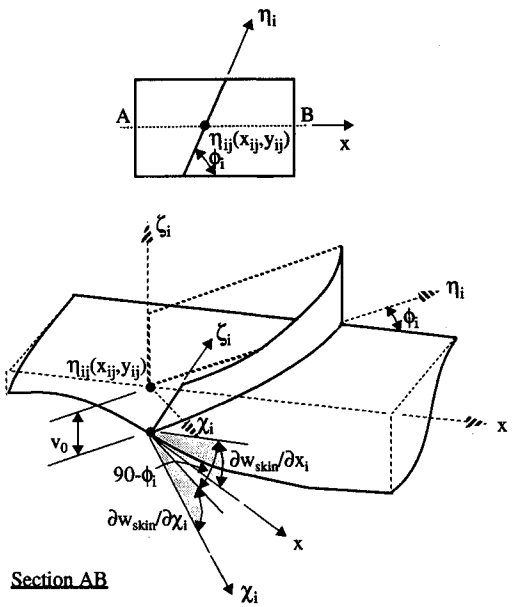

Fig. 2 Skin and stiffener deformations.

C. Final Panel Stability Equations

The Lagrangian of the system is given by

$$L = \Pi + \sum_{i=1}^{I}\sum_{j=1}^{J}\mu_{ij}g_{ij} + \sum_{i=1}^{I}\sum_{j=1}^{J}\nu_{ij}h_{ij} \tag{25}$$

where μ_{ij} and ν_{ij} are the Lagrange multipliers associated with the constraints g_{ij} and h_{ij}, respectively. The solution of the problem is given by the set of equations

$$\begin{aligned}
&\frac{\partial L}{\partial A_{mn}} = 0 \quad \begin{cases} m = 1, 2, \ldots, M \\ n = 1, 2, \ldots, N \end{cases} \\
&\frac{\partial L}{\partial B_{ik}} = 0 \quad \begin{cases} i = 1, 2, \ldots, I \\ k = 1, 2, \ldots, K \end{cases} \\
&\frac{\partial L}{\partial C_{itk}} = 0 \quad \begin{cases} i = 1, 2, \ldots, I \\ k = 1, 2, \ldots, K' \\ t = 1 \end{cases} \\
&\frac{\partial L}{\partial \mu_{ij}} = 0 \quad \begin{cases} i = 1, 2, \ldots, I \\ j = 1, 2, \ldots, J \end{cases} \\
&\frac{\partial L}{\partial \nu_{ij}} = 0 \quad \begin{cases} i = 1, 2, \ldots, I \\ j = 1, 2, \ldots, J \end{cases}
\end{aligned} \tag{26}$$

that represents a set of $(MN + IK + IK' + 2IJ)$ equations in $(MN + IK + IK' + 2IJ)$ unknowns, where $M \times N$ is the number of terms used in the skin deflection series, I is the number of stiffeners, J is the number of constraint points per stiffener, K is the number of terms used in the stiffener in-plane deflection series, and K' is the number of terms used in the stiffener out-of-plane deflection series (with only one term used in the transverse direction). These equations are given in Appendix B. This is a generalized eigenvalue problem with λ being the eigenvalue, and the undetermined coefficients and Lagrange multipliers A_{mn}, B_{ik}, C_{i1k}, μ_{ij}, ν_{ij} being

the eigenvector. In matrix form, these equations can be written as

$$\begin{bmatrix} [K_{11}] & [0] & [0] & [K_{14}] & [K_{15}] \\ [0] & [K_{22}] & [0] & [K_{24}] & [0] \\ [0] & [0] & [K_{33}] & [0] & [K_{35}] \\ [K_{41}] & [K_{42}] & [0] & [0] & [0] \\ [K_{51}] & [0] & [K_{53}] & [0] & [0] \end{bmatrix} \begin{Bmatrix} \{A\} \\ \{B\} \\ \{C\} \\ \{\mu\} \\ \{\nu\} \end{Bmatrix} = \lambda \begin{bmatrix} [M_{11}] & [0] & [0] & [0] & [0] \\ [0] & [M_{22}] & [0] & [0] & [0] \\ [0] & [0] & [M_{33}] & [0] & [0] \\ [0] & [0] & [0] & [0] & [0] \\ [0] & [0] & [0] & [0] & [0] \end{bmatrix} \begin{Bmatrix} \{A\} \\ \{B\} \\ \{C\} \\ \{\mu\} \\ \{\nu\} \end{Bmatrix} \tag{27}$$

The set of equations described above can be condensed in order to reduce computational effort. This is achieved by equating the number of terms in the in-plane deflection series of the stiffeners K, and the number of constraint points J. It is then possible to invert $[K_{24}]$ and $[K_{42}]$ to solve for the terms $\{\mu_{ij}\}$ and $\{B_{ik}\}$, before calling the solver, by using the following equations obtained from the second and the fourth "lines" of the system:

$$\begin{aligned} \{\mu\} &= [K_{24}]^{-1}(\lambda[M_{22}]\{B\} - [K_{22}]\{B\}) \\ \{B\} &= -[K_{42}]^{-1}[K_{41}]\{A\} \end{aligned} \tag{28}$$

The system is then reduced to

$$\begin{bmatrix} [K^*] & [K_{15}] & [0] \\ [K_{51}] & [0] & [K_{53}] \\ [0] & [K_{35}] & [K_{33}] \end{bmatrix} \begin{Bmatrix} \{A\} \\ \{\nu\} \\ \{C\} \end{Bmatrix} = \lambda \begin{bmatrix} [M^*] & [0] & [0] \\ [0] & [0] & [0] \\ [0] & [0] & [M_{33}] \end{bmatrix} \begin{Bmatrix} \{A\} \\ \{\nu\} \\ \{C\} \end{Bmatrix} \tag{29}$$

where

$$[K^*] = [K_{11}] + [K_{14}][K_{24}]^{-1}[K_{22}][K_{42}]^{-1}[K_{41}] \tag{30}$$

$$[M^*] = [M_{11}] + [K_{14}][K_{24}]^{-1}[M_{22}][K_{42}]^{-1}[K_{41}] \tag{31}$$

The order of the new system is $(MN + IK + IK')$.

Despite the condensation of the system, for a panel with many cells (identical groups of stiffeners lined side by side across the panel) the size of the eigenvalue problem increases very rapidly. A typical example is a 5-cell, cross-stiffened panel ($I = 10$), with $K = 13$, $K' = 6$, $T = 1$, $M = 17$, and $N = 9$. For this problem, the size of the two matrices is 343 by 343. The large size of the matrices is due mostly to the inclusion of the constraint enforcing rotational continuity of the mode shape at the bases of the stiffeners. If the problem is formulated with the out-of-plane displacement constraint only, the size of the matrices would have been only 153 by 153.

In addition to the problem size, the accuracy of the computed buckling load is influenced strongly by the number of terms in the shape functions and the number of points used to impose the two types of constraints. A method used to determine the necessary number of terms and constraints is described in Ref. 6.

III. Examples and Discussion

The effect of imposing constraints on the continuity of rotation between the skin and the stiffeners is investigated first. Results of the present analysis are compared with the results of the earlier study,[2] in which only the flexural contribution of the stiffeners was taken into account using the first constraint described in the previous section. For convenience, that method of analysis is referred to as the LMM1 (Lagrange Multipliers Method 1). The present method that also includes the rotational continuity is referred to as the LMM2 for the remainder of this article.

For the purposes of comparison, a 3-cell, cross-stiffened panel is considered. The panel is 80 in. wide, 28 in. high, and represents a typical wing-rib panel of a large transport aircraft.[7] The skin construction of the panel is a $[\pm 45/90/0]_s$ quasi-isotropic laminate, and the stiffeners are made of 0-deg fibers only. The material properties used for the analysis are; $E_1 = 18.5 \times 10^6$ psi, $E_2 = 1.64 \times 10^6$ psi, $G_{12} = 0.87 \times 10^6$ psi, $\nu_{12} = 0.3$.

The buckling load of the panel under pure compressive loads was computed using both the LMM1 and LMM2 procedures for various stiffener heights. The results are compared with the results of a finite element analysis in Table 1. The finite element program used for the analysis is the computational structural mechanics (CSM) testbed[8] (recently renamed as COMET). Although the finite element analysis is also an approximate solution for the problem, FEM results are used here as baseline results for comparison since no closed form solution is known.

As can be observed from Table 1, the LMM1 analysis predicts the buckling load of panels with small stiffener height to be much lower than the finite element results. The new

Table 1 Comparison of buckling loads for 3-cell, cross-stiffened panels

Stiffener height, in.	Panel buckling load, lbf/in.			N_{LMM1}/N_{FEM}	N_{LMM2}/N_{FEM}
	N_{FEM}	N_{LMM1}	N_{LMM2}		
0.50	573	342	471	0.60	0.82
0.75	705	613	649	0.87	0.92
1.00	748	708	727	0.95	0.97
1.25	782	743	770	0.95	0.98

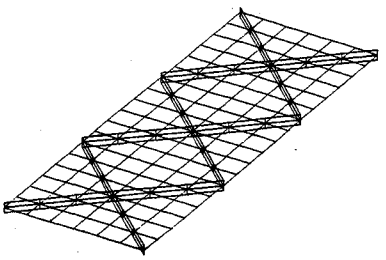

Finite Element Model

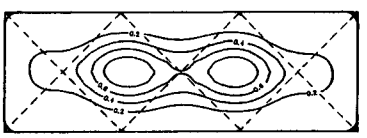

Finite Element Mode Shape

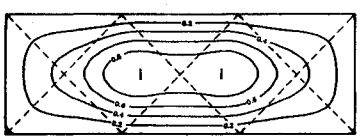

LMM1 Mode Shape

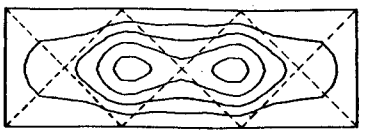

LMM2 Mode Shape

Fig. 3 Buckling mode contours of a three-cell panel.

method, on the other hand, predicts buckling loads that are much closer to the finite element results. This improvement confirms that enforcing continuity of rotation between the skin and the stiffeners has a significant effect on the predicted buckling load of the panel. For a panel with deep stiffeners, the critical load is governed by the buckling of the stiffeners in their out-of-plane direction without much participation of the skin, a mode that is already taken care of by the LMM1 analysis. However, for shallow stiffeners the critical load is controlled by the buckling of the skin in a global mode that requires participation of the stiffeners. The stiffeners in this case not only buckle in a direction perpendicular to the skin, but are also required to undergo a rotational mode due to the oblique nature of the stiffeners. This effect is more accurately modeled by the present analysis. For example, contour plot of the buckling modes of the panel with a stiffener height of $h = 0.5$ in. are shown in Fig. 3 for the three analysis. Also shown in the figure is the finite element model of the panel. The model consists of 180 nine-noded quadrilateral shell elements, including the 72 shell elements used to model the stiffeners. Efficiency of the present method can be assessed based on the size of the eigenvalue problem that needs to be solved. For this particular problem of a three-cell panel, the LMM1 and LMM2 analyses have 153 and 267 DOF, respectively. The finite element model, on the other hand, has over 4000 DOF, which is approximately a 15-fold increase in the size of the eigenvalue problem compared to the LMM2 analysis. The predicted mode shape by the LMM2 analysis is clearly closer to the finite element prediction than the LMM1 analysis and, despite the increase in computational requirement from LMM1 analysis to LMM2, both LMM1 and LMM2 analysis are computationally much more efficient than the finite element analysis.

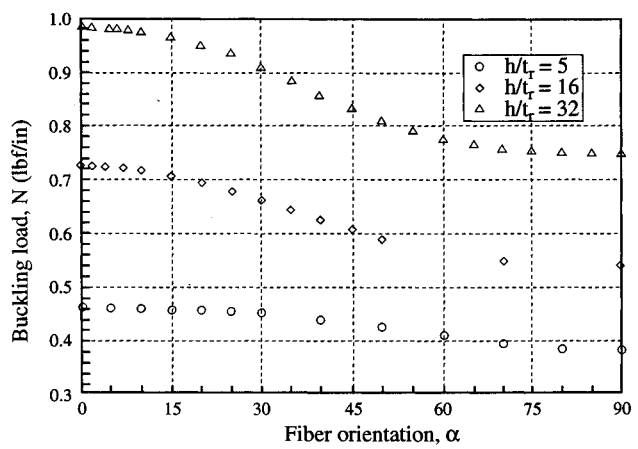

Fig. 4 Effect of stiffener lamination $[\pm\alpha/0_2]_s$ on buckling load of a thick skin ($t_s = 0.256$ in.) panel.

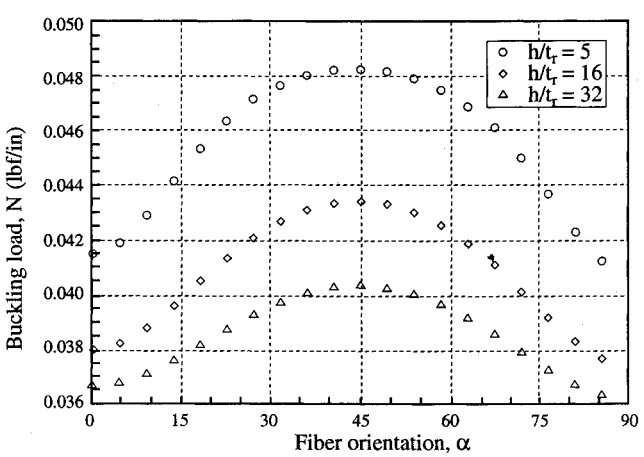

Fig. 5 Effect of stiffener lamination $[\pm\alpha/0_2]_s$ on buckling load of a thin skin ($t_s = 0.08$ in.) panel.

A. Laminated Stiffeners

Modeling the stiffeners as plate elements in the LMM2 analysis allows us to change and possibly optimize the lamination stacking sequence of the stiffeners. Therefore, we next study the effect of the stiffener stacking sequence on the buckling load by including some angle plies on the two faces of the stiffeners. The stiffener stacking sequence is changed to $[\pm\alpha/0_2]_s$, where α is varied from 0 to 90 deg. Nine basic configurations of a 1-cell, cross-stiffened panel are considered. The nine basic configurations are divided into three groups. The first group has a thick skin ($t_s = 0.256$ in.), the second one has a thin skin ($t_s = 0.08$ in.), and the third one has a medium skin thickness ($t_s = 0.15$ in.). In each group, three different stiffener-height to stiffener-thickness ratios ($h/t_r = 5$, $h/t_r = 16$, $h/t_r = 32$) are investigated. The cross-sectional aspect ratio of the stiffener is changed by changing both the stiffener height h and the stiffener thickness t_r such that the cross-sectional area of the stiffeners remains constant ($ht_r = 0.4084$). Therefore, the same load distribution between the stiffener and skin is preserved from one configuration to another within a given group.

Buckling load results for the three groups of panels are shown in Figs. 4–6 as functions of the ply angle α. For the thick skin panel (Fig. 4), the highest buckling load is achieved for panels with 0-deg (unidirectional) fiber stiffeners regardless of the stiffener aspect ratio (h/t_r). Moreover, the larger the stiffener aspect ratio, the higher is the panel buckling load for any angle α. For this thick-skin panel, most of the applied loads are carried by the skin, and the overall buckling of the panel is critical. Therefore, increasing the stiffener aspect ratio increases the overall bending stiffness and the buckling load.

For the thin skin panel (Fig. 5) the effect of the stiffener out-of-plane bending stiffnesses seems to become a critical factor in the buckling of the panel. Unlike the previous cases where a large stiffener aspect ratio increases the buckling load, a higher aspect ratio for the thin skin panel lowers the panel buckling load. Moreover, the stiffener ply angle α at which the largest buckling load is reached corresponds to $\alpha = 45$ deg, regardless of the stiffener aspect ratio. For these panels, a larger fraction of the applied load is carried by the stiffeners, and the local buckling of the stiffeners dominates the critical load of the panel.

The panels with a medium skin thickness (Fig. 6) demonstrate two interesting points. First, for each aspect ratio there is an angle α for which the buckling load is maximum. This indicates that both the out-of-plane bending and in-plane extensional stiffnesses of the stiffeners are important, and that by judiciously laminating the stiffeners it is possible to achieve

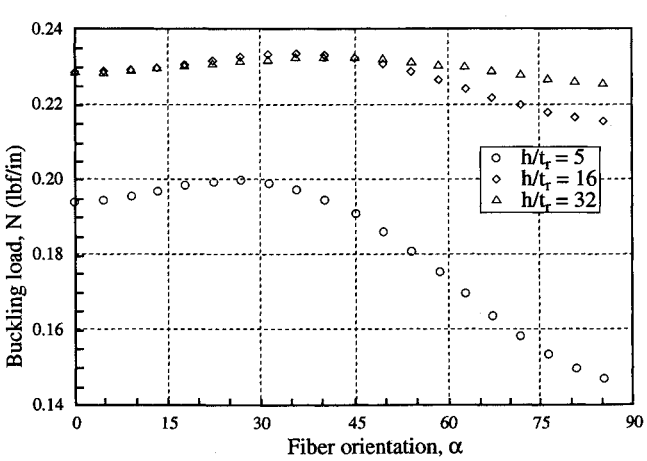

Fig. 6 Effect of stiffener lamination $[\pm\alpha/0_2]_s$ on buckling load of a medium skin thickness ($t_s = 0.15$ in.) panel.

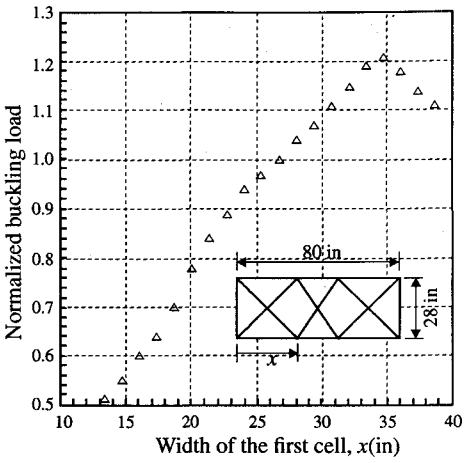

Fig. 7 Effect of cell distribution on the buckling load of a panel.

gains in the buckling load for the same panel weight. For example, with $\alpha = 27$ deg, the buckling load of the panel with a stiffener aspect ratio of $h/t_s = 5$ is increased by about 5% over the same panel with all 0-deg stiffeners. The second interesting point is that the two curves corresponding to the stiffener aspect ratios of 16 and 32 are very close together. That is, the buckling load remains the same, although the aspect ratio of the stiffeners is doubled from $h/t_r = 16$ to $h/t_r = 32$.

B. Optimal Cell Distribution

By keeping the panel width constant and varying the cell width, it is possible to notably increase the buckling load of a panel. As an example, a 3-cell, cross-stiffened panel under in-plane compression loading is considered where the width of its first cell is a variable. The width of the remaining two cells can be computed from symmetry. The cells are equally sized when their width is 26.66 in. The buckling load of the panel, normalized by the buckling load of a uniform grid panel, is shown in Fig. 7 as a function of the first cell width. From Fig. 7 it appears that the buckling load of this panel is the highest for a first cell width of about 35 in., which corresponds to a narrow cell in the middle and two wide cells on the sides. The maximum buckling load is as much as 20% larger than that of the uniform grid panel.

IV. Concluding Remarks

A computationally efficient buckling and strength analysis procedure that can be used for the preliminary design of grid-stiffened flat panels is developed. The analysis is a modified version of an earlier approach that uses the Rayleigh-Ritz method coupled with the Lagrange multiplier technique. The stiffeners are modeled as plate elements, as opposed to the beam elements used earlier, and the buckling mode shapes are assumed independently for the skin and stiffeners. Compatibility of the skin and stiffener deformations at buckling is enforced at selected locations via constraints in the Lagrange multiplier technique. These constraints include the compatibility of the skin out-of-plane mode and the stiffener in-plane mode, and the compatibility of the skin rotation and the stiffener rotation at the skin-stiffener connections. It was demonstrated, through comparison with finite element results, that the new more comprehensive analysis results in a more accurate calculation of the panel buckling loads, especially in the case of stiffeners with small heights compared to the thickness of the skin.

The capability of modeling the stiffeners as plate elements attached to the skin also enables the designer to consider laminated stiffeners. The effects of the in-plane and out-of-plane bending stiffness of the stiffeners on panel buckling load is evaluated by parametrically changing the lamination angle of the stiffeners and stiffener cross-sectional aspect ratio. For most configurations, laminate orientation angle is found to have a substantial effect on the critical load of a panel. It was demonstrated that the optimal stiffener is not always unidirectional, and tailoring the stiffener ply sequence can lead to improvement in panel stability.

The new analysis presented also includes a capability for considering panels with variable stiffener grid density. It was demonstrated that panels with a variable grid density can lead to designs with improved buckling performance compared to uniform density panels.

Appendix A: Energy Coefficients

$$P^{mn} = \frac{\pi^4 ab}{8}\left[D_{11}\left(\frac{m}{a}\right)^4 + 2(D_{12} + 2D_{66})\left(\frac{mn}{ab}\right)^2 + D_{22}\left(\frac{n}{b}\right)^4\right]$$

$$Q^{ik} = \frac{\pi^4 E_1 I_s}{4l_i^3} k^4$$

$$R^{mn} = \frac{\pi^2 ab}{8}\left[\overline{N}_x\left(\frac{m}{a}\right)^2 + \overline{N}_y\left(\frac{n}{b}\right)^2\right]$$

$$S^{mnpq} = \begin{cases} \overline{N}_x \dfrac{4mnpq}{(p^2 - m^2)(n^2 - q^2)} & \text{for } (m + p) \text{ and } (n + q) \text{ odd} \\ 0 & \text{otherwise} \end{cases}$$

$$T^{ik} = \frac{\pi^2 k^2 h}{2l_i}\overline{N}_i$$

$$U^{itkp} = U_{11}^{itkp} + U_{12}^{itkp} + U_{22}^{itkp} + U_{66}^{itkp}$$

$$U_{11}^{itkp} = \frac{D_{11}\pi^4}{2l_i^3}\frac{k^4}{t + p + 1}[(t_s + h)^{t+p+1} - t_s^{t+p+1}]\eta_t^p$$

$$U_{12}^{itkp} = -\frac{D_{12}\pi^2}{l_i}k^2 p(p - 1)\frac{1}{t + p + 1}[(t_s + h)^{t+p-1} - t_s^{t+p-1}]\eta_t^p$$

$$U_{22}^{itkp} = \frac{D_{22}l_i}{2}tp(t - 1)(p - 1)\frac{1}{t + p - 3}[(t_s + h)^{t+p-3} - t_s^{t+p-3}]\eta_t^p$$

$$U_{66}^{itkp} = \frac{2D_{66}\pi^2}{l_i}tp\frac{k^2}{t + p - 1}[(t_s + h)^{t+p-1} - t_s^{t+p-1}]\eta_t^p$$

$$V^{itkp} = \frac{\overline{N}_i\pi^2}{2l_i}\frac{k^2}{t + p + 1}[(t_s + h)^{t+p+1} - t_s^{t+p+1}]\eta_t^p$$

$$\eta_t^p = \frac{[1 + (-1)^{t+p}]}{2}$$

and $t + p \geq 4$ in the summation for the term U_{22}^{itkp}.

Appendix B: Final Panel Stability Equations

$$m = 1, 2, \ldots, M$$

$$n = 1, 2, \ldots, N$$

$$2A_{mn}P^{mn} + \sum_{i=1}^{I}\sum_{j=1}^{J} \mu_{ij}\left(\sin\frac{m\pi x_{ij}}{a}\sin\frac{n\pi y_{ij}}{b}\right) + \sum_{i=1}^{I}\sum_{j=1}^{J} \nu_{ij}\left(-\frac{m\pi}{a}\sin\phi_i\cos\frac{m\pi x_{ij}}{a}\sin\frac{n\pi y_{ij}}{b} + \frac{n\pi}{b}\cos\phi_i\sin\frac{m\pi x_{ij}}{a}\cos\frac{n\pi y_{ij}}{b}\right) - \lambda\left(2A_{mn}R^{mn} + 2\sum_{p=1}^{M}\sum_{q=1}^{N} A_{pq}S^{mnpq}\right) = 0$$

$$i = 1, 2, \ldots, I$$

$$k = 1, 2, \ldots, K$$

$$\left(2B_{ik}Q^{ik} - \sum_{j=1}^{J} \mu_{ij}\sin\frac{k\pi\eta_{ij}}{l_i} - \lambda(2B_{ik}T^{ik}) = 0\right)$$

$$i = 1, 2, \ldots, I$$

$$t = 1, 2, \ldots, T \qquad (T = 1)$$

$$k = 1, 2, \ldots, K'$$

$$\left(2\sum_{p=1}^{T} C_{ipk}U_{ilkp} - \sum_{j=1}^{J} \nu_{ij}\sin\frac{k\pi\eta_{ij}}{l_i} = 2\lambda\sum_{p=1}^{T} C_{ipk}V_{ilkp}\right)$$

$$i = 1, 2, \ldots, I$$

$$j = 1, 2, \ldots, J$$

$$\left(\sum_{m=1}^{M}\sum_{n=1}^{N} A_{mn}\sin\frac{m\pi x_{ij}}{a}\sin\frac{n\pi y_{ij}}{b} - \sum_{k=1}^{K} B_{ik}\sin\frac{k\pi\eta_{ij}}{l_i} = 0\right)$$

$$i = 1, 2, \ldots, I$$

$$j = 1, 2, \ldots, J$$

$$\sum_{m=1}^{M}\sum_{n=1}^{N} A_{mn}\left[-\frac{m\pi}{a}\sin\phi_i\cos\frac{m\pi x_{ij}}{a}\sin\frac{n\pi y_{ij}}{b} + \frac{n\pi}{b}\cos\phi_i\sin\frac{m\pi x_{ij}}{a}\cos\frac{n\pi y_{ij}}{b}\right] + \sum_{k=1}^{K'} C_{i1k}\sin\frac{k\pi\eta_{ij}}{l_i} = 0$$

Acknowledgments

This research was supported in part by NASA Grant NAG-1-643. The first author appreciates the support provided by the Aircraft Structures Branch of NASA Langley Research Center, Hampton, Virginia.

References

[1]Gürdal, Z., and Gendron, G., "Optimal Design of Geodesically Stiffened Composite Cylindrical Shells," *Composites Engineering*, Vol. 3, No. 12, 1993, pp. 1131–1147.

[2]Phillips, J. L., and Gürdal, Z., "Analysis and Optimum Design of Geodesically Stiffened Composite Panels," *Composite Material Design and Analysis*, edited by W. P. de Wilde and W. R. Blain, Computational Mechanics Publications, Springer-Verlag, New York, 1990, pp. 509–528.

[3]Rivello, R. M., *Theory and Analysis of Flight Structures*, McGraw-Hill, New York, 1969.

[4]Whitney, J. M., *Structural Analysis of Laminated Anisotropic Plates*, Technomic Publishing, Lancaster, PA, 1987.

[5]Grall, B., and Gürdal, Z., "Structural Analysis and Design of Geodesically Stiffened Composite Panels with Variable Stiffener Distribution," Center for Composite Materials and Structures, Virginia Polytechnic Inst. and State Univ., CCMS-92-24, VPI-E-92-21, Blacksburg, VA, Aug. 1992.

[6]Phillips, J. L., and Gürdal, Z., "Structural Analysis and Optimum Design of Geodesically Stiffened Composite Panels," Center for Composite Materials and Structures, Virginia Polytechnic Inst. and State Univ., CCMS-90-05, Blacksburg, VA, July 1990.

[7]Swanson, G. D., and Gürdal, Z., "Structural Efficiency Study of Graphite-Epoxy Aircraft Rib Structures," *Journal of Aircraft*, Vol. 27, No. 12, 1990, pp. 1011–1020.

[8]Stewart, C. B., *Computational Structural Mechanics Testbed User's Manual*, NASA-TM-100644, Washington, DC, Oct. 1989.